A 36µW 1.1mm^2 Reconfigurable Analog Front-End for Cardiovascular and Respiratory Signals Recording

Jiawei Xu, Mario Konijnenburg, Hyunsoo Ha, Roland van Wegberg, Shuang Song, Dolores Blanco-Almazán, Chris Van Hoof, and Nick Van Helleputte

***Abstract*—This paper presents a 1.2V 36µW reconfigurable analog front-end (R-AFE) as a general-purpose low-cost IC for multiple-mode biomedical signals acquisition. The R-AFE efficiently reuses a reconfigurable preamplifier, a current generator (CG), and a mixed signal processing unit, having an area of 1.1mm^2 per R-AFE while supporting 5 acquisition modes to record different forms of cardiovascular and respiratory signals. The R-AFE can interface with voltage-, current-, impedance- and light-sensors and hence can measure electrocardiography (ECG), bio-impedance (BioZ), photoplethysmogram (PPG), galvanic skin response (GSR), and general-purpose analog (GPA) signals. Thanks to the chopper preamplifier and the low-noise CG utilizing dynamic element matching (DEM), the R-AFE mitigates 1/*f* noise from both the preamplifier and the CG for improved measurement sensitivity. The IC achieves competitive performance compared to the state-of-the-art dedicated readout ICs of ECG, BioZ, GSR and PPG, but with approximately 1.4x-5.3x smaller chip area per channel.**

***Index Terms*—reconfigurable, cardiovascular, respiratory, bio-impedance, multi-mode, dynamic element matching, ECG, GSR.**

I. Introduction

THE long-term monitoring of cardiovascular and respiratory signs in a wearable format is a practical solution to improve user's comfort and the diagnostic quality of chronic conditions. Two examples are congestive heart failure and obstructive sleep apnea. These chronic diseases are often characterized by high blood pressure, arrhythmias, respiratory disorders, body fluid overload, or even a heart attack. Therefore, low-power and miniaturized biomedical ICs that continuously measure these vital signs with medical-grade quality will improve chronic disease management and enable preventive healthcare.

Many wearable medical ICs only focus on the acquisition and optimization of single vital sign for dedicated applications, such as electrocardiography (ECG) [1], bio-impedance (BioZ) [2], photoplethysmogram (PPG) [3] and so on. Integrating several ICs on the system level to enrich the bio-parameter matrix is not compact nor power-efficient. A multi-sensor ASIC (Fig. 1) [4] solves this problem by integrating several dedicated readout channels on a single chip. However, this often requires a large chip area (>10mm^2) and thus being expensive and less flexible. The reconfigurable AFEs (R-AFEs) [6][7] measure multimodal (bio-)signals while still being compact and low cost. They show promising results but the remaining challenges are performance optimization of noise, power dissipation and reconfigurability

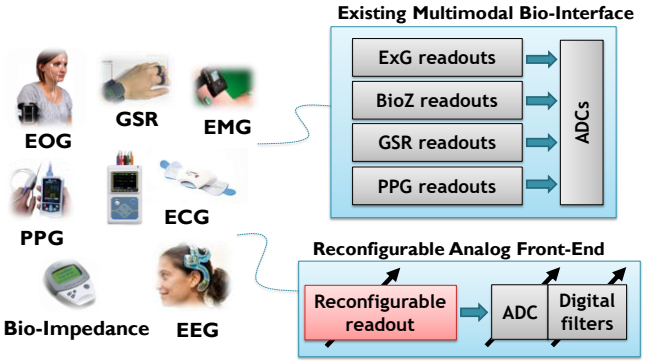

Fig. 1. Multimodal vital signs acquisition with dedicated readout channels or a reconfigurable readout channel

to meet the medical compliance [8].

This paper presents a low-power R-AFE for multimodal bio-signal acquisition [9]. It is highly reconfigurable among five acquisition modes, i.e., ECG mode for biopotential signals like ECG and EEG; BioZ mode for impedance cardiography (ICG) and respiration; galvanic skin response (GSR) mode for skin conductance representing cognitive state; PPG mode to detect blood oxygen saturation, heart rate and cardiac cycle; general-purpose analog (GPA) mode for other types of voltage inputs, e.g., a body temperature sensor, or a microphone to record body sounds (e.g. heartbeat, breathing). Apart from the multimodal recording, the R-AFE utilizes dynamic circuit techniques in the key building blocks to reduce 1/*f* noise for better sensitivity.

II. Architecture Overview

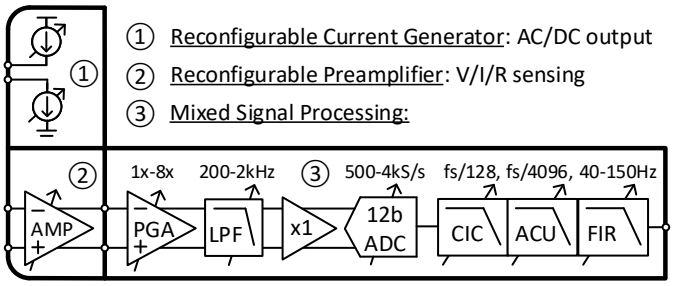

Fig. 2. Architecture of the reconfigurable analog-front-end (R-AFE) for multi-mode bio-signal acquisition

The R-AFE (Fig. 2) includes a reconfigurable preamplifier, a low-noise current generator (CG), followed by a mixed signal processing chain to set channel settings, such as voltage gain,

J. Xu, M. Konijnenburg, H. Ha, R. van Wegberg are with Holst Centre/imec, Eindhoven, 5656AE, The Netherlands (e-mail: jiawei.xu@imec-nl.nl).

D. Blanco is with Institute for Bioengineering of Catalonia (IBEC), 08028, Barcelona, Spain.

C. Van Hoof, S. Song and N. Van Helleputte are with imec, Heverlee, 3001, Belgium.

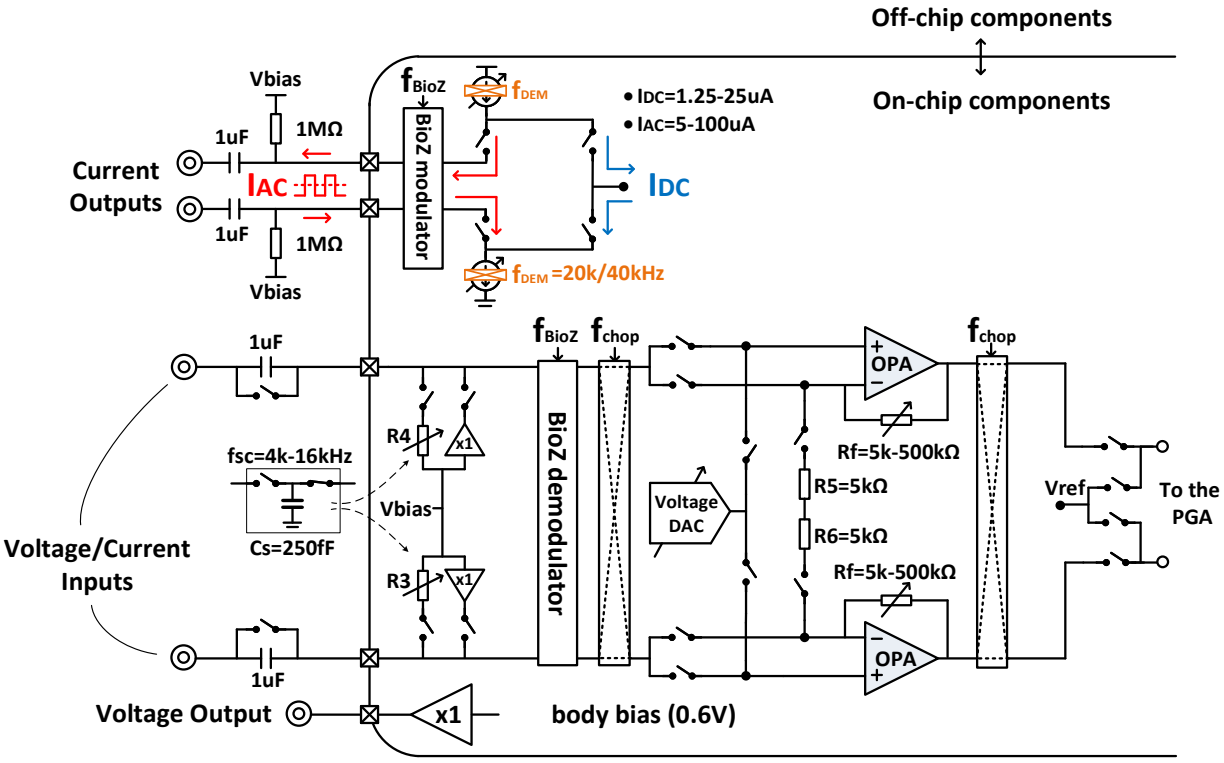

Fig. 3. Block diagram of the reconfigurable amplifier and the current generator

bandwidth, dynamic range and (over-)sampling rate, to support the multimodal acquisition.

As the heart of the R-AFE, the preamplifier must ensure high quality acquisition in all modes while reusing core components efficiently to reduce chip area. The preamplifier (Fig. 3) is built on non-inverting resistive feedback because it provides inherent high input-impedance and enhanced common-mode rejection ratio (CMRR). In addition, it can be easily reconfigured to two transimpedance amplifiers (TIAs) for current sensing in GSR and PPG mode. 1/*f* noise is used to be a dominant noise source limiting the sensitivity of biopotential signals measurement. To remedy this issue, this IC utilizes dynamic circuit techniques, such as chopping [10] and dynamic element matching (DEM) [11], in ECG, GPA and BioZ modes.

One of the major design challenges of a reconfigurable pre-amplifier is to ensure that the core components, i.e. operational amplifier (OPA), feedback networks and input bias network, can be reconfigured among different acquisition modes without degrading the performance. Any real switch will exhibit a finite off-resistance and non-zero on-resistance. Especially when the non-ideal switches appear on the sensitive input lines, this will negatively impact critical analog performance metrics like input impedance, noise, gain accuracy, CMRR, cut-off frequency. It is important that, among different modes, the total number of switches connected in series is minimized to reduce their finite on-resistance, the associated voltage noise and gain error while maximizing the off-resistance. Therefore, each static switch for reconfiguration is implemented as a transmission gate (TG) in a body grabbing (BG) scheme to further reduce its on-resistance (Fig. 4) [12]. Via M3, the bulk of the switch M2 is "grabbed" by the input common-mode (CM) signal during the "ON" state for a low threshold voltage V_T. The same bulk is then driven by V_{DD} via M4 during the "OFF" state to minimize the leakage current. The simulation of the body grabbing switch shows an on-resistance spread between 13-202Ω and an off-resistance of more than 2.47GΩ over the process, voltage and temperature (PVT) variations, and different CM levels (V_{CM}=200mV to 1V, V_{DD}=1.08-1.35V, T=-10-85°C).

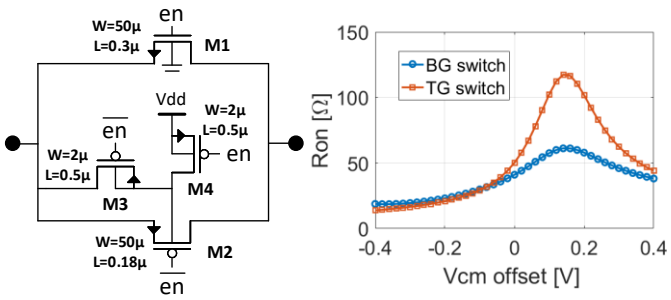

Fig. 4. Body grabbing (BG) switch shows lower on-resistance compared to a transmission gate (TG) switch

A. ECG and General-Purpose Analog (GPA) Mode

ECG has been a classical non-invasive approach to diagnose cardiovascular diseases, like arrhythmias, carditis, myocardial ischemia and infarction. The biopotential ECG is often recorded by a differential amplifier through a pair of electrodes placed on the chest or on the wrist. The major specifications of an ECG amplifier include low noise, large input impedance and a high CMRR [8].

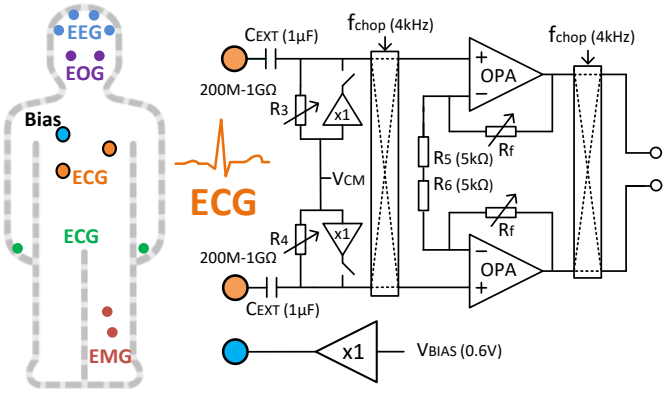

Fig. 5. ECG acquisition mode

To meet these requirements, the preamplifier is configured as an AC-coupled chopper instrumentation amplifier (IA) with a resistive feedback (Fig. 5). Apart from a high input-impedance, this chopper IA also exhibits a CMRR of more than 100dB. The input CM voltage is fed forward to the input balancing resistors (R_5, R_6) through two OPAs, which nulls the input CM current across R_5, R_6 and R_f. Both the OPAs can thus tolerate large CM signals without clipping. Furthermore, to cope with ill-defined differential-mode interference or artifacts, the OPA should have a rail-to-rail voltage headroom at both input and output. These requirements are fulfilled by a complementary input pair and a translinear loop-based class-AB output (Fig. 6) [13]. Both R_5 and R_6 are fixed to 5kΩ for noise specification, and the class-AB output stage is able to drive a 5kΩ feedback resistor R_f at the lowest IA gain of 2. Although even smaller resistors would reduce the noise further, this is subject to increased power.

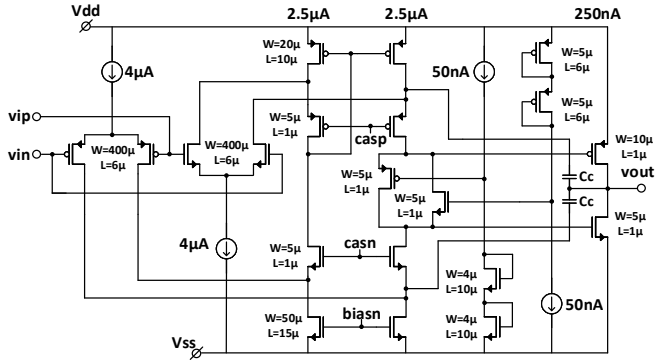

Fig. 6. Core OPA with rail-to-rail input and class-AB output

A high-pass filter (HPF) (Fig. 5) placed prior to the chopper IA rejects any electrode offset. This HPF has a <0.01Hz cutoff frequency, which is reconfigurable through switched-capacitor bias resistors (R_3, R_4 in Fig. 3). Although up to 20% mismatch between input coupling capacitors may exist, R_3 and R_4 (200M-1GΩ) reduce the voltage drop over C_{EXT}. This helps the IA to maintain a CMRR of 100dB and input-impedance of 140MΩ, both at 50Hz. The input referred noise of the ECG preamplifier is expressed as:

$$\overline{V_{n,ECG}^2} = 2 \times \left(\overline{v_{n,OPA}^2} + 4kTR_5 + \frac{kT}{R_3 \pi^2 f_i^2} \right) \quad (1)$$

where three terms in the equation are attributed to the OPA, the balancing resistor and the HPF, respectively.

Although the AC-coupled IAs compensate electrode offset and thus relaxing the input dynamic range, which positively impacts the power consumption, their main drawback is a very long settling time, typically in the order of a few tens of seconds due to the large RC time constant of the HPF. To overcome this issue, two analog buffers (Fig. 5) connected in parallel with R_3 and R_4 allow fast settling (<500ms). These buffers are powered off during normal ECG acquisition.

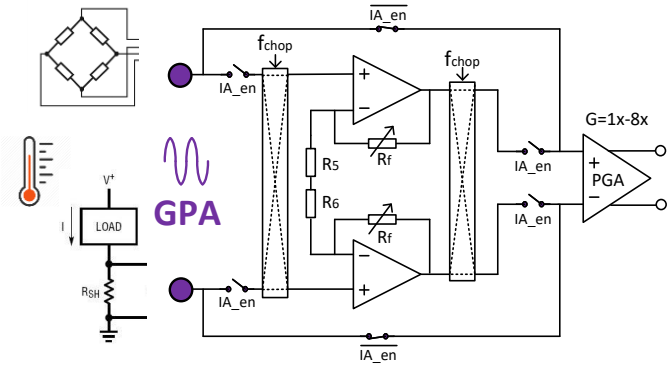

Fig. 7. GPA acquisition mode

In GPA mode (Fig. 7), the preamplifier interfaces with other general sensors with analog outputs, like a temperature sensor for body temperature sensing, or a microphone to record body sounds. These sensors may output a DC component, so the HPF before the preamplifier can be bypassed. In addition, since these general sensors may have less noise requirement than the ECG, the IA can be bypassed too to save power. This makes the PGA the input stage and it reduces the total GPA channel power from 33µW to 17.3µW at the cost of increased noise (Fig. 8).

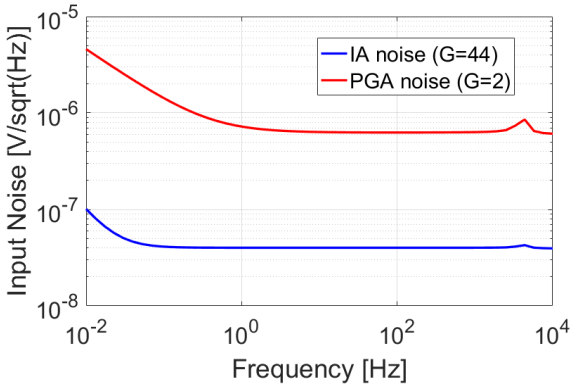

Fig. 8. Input referred noise of IA (G=44) and PGA (G=2)

The PGA is built on a current-balancing chopper amplifier [4] (Fig. 9). The input balancing resistor R_i is configurable between 55k-to-440kΩ for multiple IA gain settings, and the bias current is 3µA. Since the input noise and input range are largely defined by R_i, the PGA can trade input dynamic range and noise from $120mV_{pp}/1.94\mu V_{rms}$ to $650mV_{pp}/ 12\mu V_{rms}$ in a 100Hz BW.

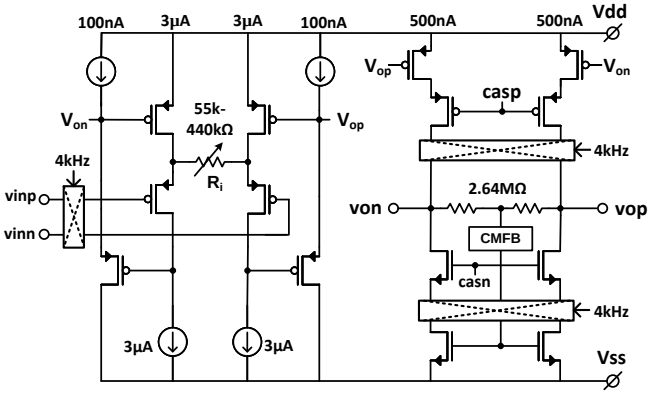

Fig. 9. Chopper PGA based on a current balancing amplifier

B. *Bio-Impedance (BioZ) Mode*

BioZ measurement is a primary approach for the diagnosis of congestive heart failure (CHF), a chronic but fatal heart disease characterized by fluid overload in the lungs. While combining the cardiac impedance with the ECG can also gain insight into sympathetic nervous system influence, such as stroke volume and cardiac output.

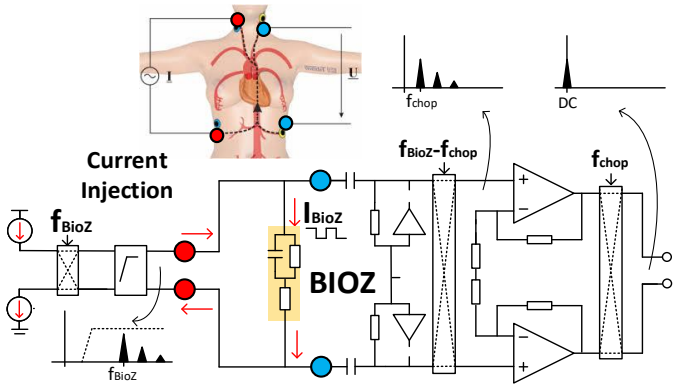

Fig. 10. BioZ acquisition mode

BioZ is usually measured with 4 electrodes (Fig. 10), where two for current excitation and the other two for voltage sensing. The CG provides a differential output current (with both sink and source) in square or sinusoidal wave. This AC current flows through BioZ between two sensing electrodes and the resulting voltage across BioZ is amplified by the IA. In this work, the CG provides a current magnitude of 5µ-100µA_{pk} and a frequency between 1k-1MHz, which falls in the typical BioZ range while still complying with the safe current limit [14]. Fig. 11 shows the noise sources model of the BioZ channel. As a key design parameter, the sensitivity of BioZ is derived as follows:

$$\overline{R_{n,BioZ}^2} = \frac{\overline{v_{n,IA}^2} + 8kTR_E + \overline{i_{n,IA}^2}\left(R_{BioZ} + 2R_E\right)^2 + \overline{i_{n,CG}^2}R_{BioZ}^2}{I_{CG}^2} \quad (2)$$

$$\overline{R_{n,BioZ}^2}\Big|_{R_E=0} = \frac{\overline{v_{n,IA}^2} + \left(\overline{i_{n,IA}^2} + \overline{i_{n,CG}^2}\right)R_{BioZ}^2}{I_{CG}^2}$$

where $v_{n,IA}$ and $i_{n,IA}$ are the input referred voltage and current noise of the IA, respectively; R_E and R_{BioZ} are electrode-tissue impedance and bio-impedance, respectively; $i_{n,CG}$ is the current noise of the CG.

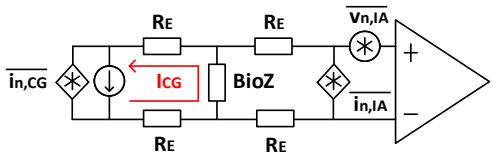

Fig. 11. Noise model of the BioZ

The equations indicate that BioZ sensitivity is determined by both the voltage noise of the IA and the current noise of the CG. When I_{CG} increases, the BioZ sensitivity is improved and the CG's current noise becomes a more dominant noise source. On the other hand, when electrodes-skin interface exhibits a large impedance R_E (e.g. dry electrode interface), the BioZ sensitivity degrades significantly because I_{CG} has to be reduced to maintain the CG's output dynamic range. The voltage noise of the IA becomes dominant and R_E also contributes more thermal noise.

However, prior-art BioZ acquisition ICs [2][4][15][16] did not take the CG's current noise into consideration. 1/*f* noise of the CG can severely reduce the BioZ sensitivity because most BioZ activities (e.g., respiration, body fluid change, ICG) fall into a bandwidth of less than 10Hz. In this work, the CG's 1/*f* current noise is reduced by dynamic element matching (DEM), where unit current mirrors of the CG are swapped sequentially at a frequency of f_{DEM} (Fig. 12) [17], thus the 1/*f* noise of each current mirror is upmodulated to $f_{DEM}/(N+1)$, where N is the current gain. Fig. 13 shows the DEM implementation of PMOS current mirrors with N=5. Each current branch has an identical magnitude and is switched between I_{ref} and I_{out} in a barrel shifter sequence.

The barrel shifter switching and current mismatch between all current branches cause spikes and ripples (Fig. 13). The spikes have its fundamental frequency at f_{DEM}, while the ripples have fundamental frequencies at $f_{DEM}/2$ and $f_{DEM}/(N+1)$. Both these aggressor signals appear at the output of the BioZ channel after CG modulation (f_{BioZ}) and IA demodulation (f_{BioZ}-f_{chop}, f_{chop}). However, they will be suppressed by the anti-aliasing low-pass filter (LPF).

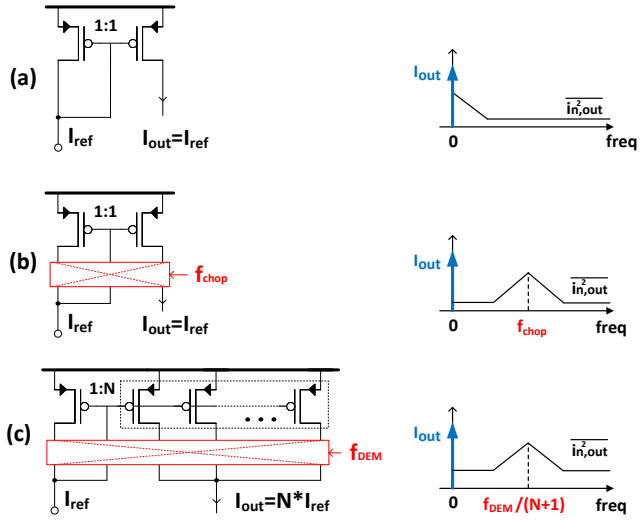

Fig. 12. Current noise characteristic a) current mirror, b) chopped current mirror and c) DEM-based current mirror

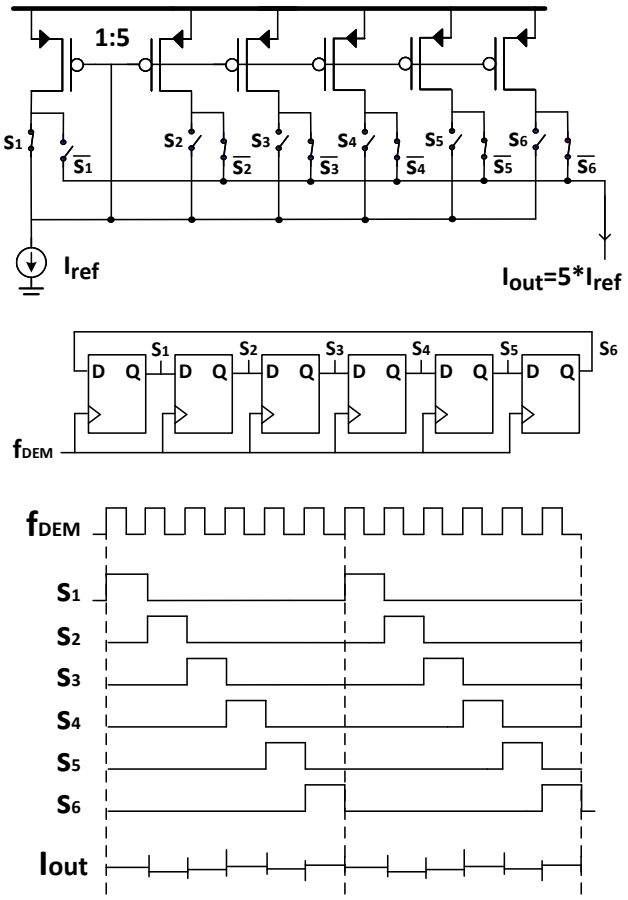

Fig. 13. CG implementation (current source) and timing diagram of the DEM with an input/output current ratio of 1:5

To convert a 50nA reference current to the output current of 100µA without using a huge N, a two-step conversion is utilized (Fig. 14). The first conversion consists of three-stage current mirrors with ratios of 1:5, 1:5 and 1:4. The 50nA current is thus amplified sequentially to 250nA, 1.25µA, and 5µA. A dummy unit current branch is added to the last stage to ensure the same ratio of 1:5 and thus simplify the DEM's clock generation. The second conversion employs variable-gain current mirrors to convert the 5µA to an output current of 5µ-to-100µA. Thus, N=1 to 20 depending on the desired magnitude of BioZ current. The two-step DEM conversion upmodulates 1/*f* noise of the CG to two frequencies at $f_{DEM}/6$ and $f_{DEM}/(N+1)$, where f_{DEM} is selected to be 20kHz or 40kHz. This ensures that the modulated 1/*f* noise, as well as DEM-induced spikes and ripples, are filtered by the LPF even when N has the maximum value of 20.

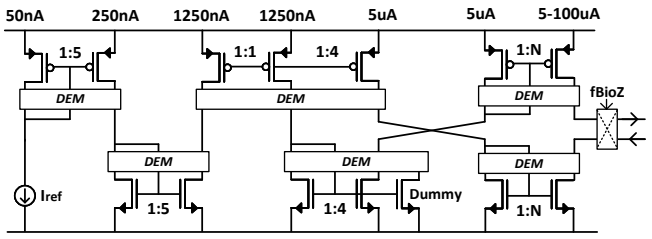

Fig. 14. DEM-based low noise current generator (CG)

One of the practical concerns is the output biasing of the CG. The output CM level of the CG may fluctuate due to electrode offset. This reduces the CG's compliance voltage dramatically, leading to a low output headroom or even saturation. To solve this issue, a RC-based HPF (Fig. 3) is inserted at the CG output to block DC offset and provides the biasing voltage at $V_{DD}/2$.

Another problem is mismatch between the sink and the source currents. Fig. 15 shows the simulated output currents of the CG over PVT corners, where supply voltage boundaries are 1.08V and 1.35V, temperature range is between -10°C to 85°C. Over PVT corners, the CG shows less than 1% current variation with respect to the 10µA reference. In case the CG has a high output impedance, the pull and push currents will try to balance each other by shifting the CG's output CM level, which reduces the compliance voltage too. Hence, two bias resistors of 1MΩ are enabled (Fig. 3) to stabilize the output compliance voltage and output impedance of the CG.

Prior-art BioZ ICs also suffer from a tradeoff between BioZ measurement frequency and power dissipation. The modulated BioZ input voltage (1k-1MHz) across BioZ would require a significant bandwidth and a power-hungry IA [2][4][5][15]. In this work, the required bandwidth and power of the IA are reduced by pre-demodulating the BioZ signal to the chopping frequency (f_{chop}) before it enters the core IA (Fig. 10) [16]. The main problem of a demodulator is that is tends to reduce the input impedance while increasing the noise due to additional switch on-resistance (similarly as chopping). To mitigate these effects, the IA's input chopper and the BioZ input modulator are merged into one block clocked by $f_{MT}=f_{BioZ}-f_{chop}$ [16].

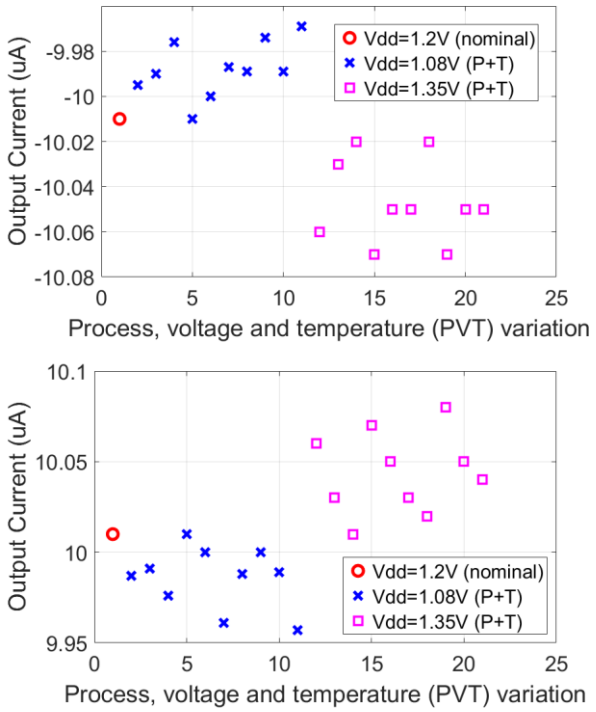

Fig. 15. CG output currents over the PVT corners: (top) current source, and (bottom) current sink. P+T refers to process (SS, SF, FS, FF) and temperature variations (-10-85ºC)

C. Galvanic Skin Response (GSR) Mode

To measure electrodermal activities, such as the amount of sweat secretion, the galvanic skin conductivity is obtained by applying a known DC voltage differential to the skin and then measuring the current response. Hence, the preamplifier in the GSR mode is reconfigured as a TIA for current sensing (Fig. 16). A voltage source (V-DAC) generates the DC voltage (ΔV) from ±50mV to ±400mV between the sensing electrode and the bias electrode via the TIA's virtual ground. A DC current (I_{GSR}) proportional to skin conductance is converted to a DC voltage by the TIA.

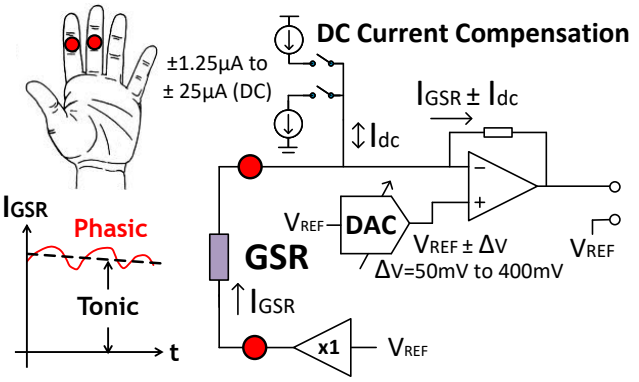

Fig. 16. GSR acquisition mode

Input dynamic range is a key challenge for a GSR readout. The GSR has both tonic (<4Hz) and phasic components (>4Hz). The tonic GSR behaves as a near-DC signal that slowly varies from tens of seconds to a few minutes and is generally related to skin hydration and psychological state. The phasic GSR is a low frequency AC signal related to cognitive processes, such as anticipation, decision making. Since the tonic level (10-50µS) is much larger than the phasic response, this usually requires a readout circuit with more than 80dB dynamic range. To reach this target without compromising the TIA's gain, DC current compensation is implemented by reconfiguring the CG in a DC mode and reconnecting it to the TIA input, as shown in Fig. 16. Since the typical I_{GSR} is less than 10µA, the CG magnitude in GSR mode is reduced to 1.25µ-25µA. Tonic GSR signal below 4Hz is low-pass filtered in digital domain through a cascaded filter chain (see section II-E).

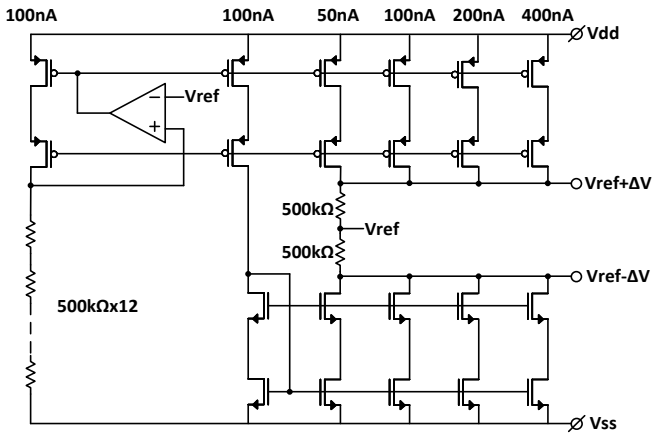

Fig. 17. GSR V-DAC schematic

Other design challenges are the voltage noise and accuracy of the GSR V-DAC, which can be significant degraded due to the single-ended TIA architecture. The V-DAC (Fig. 17) generates either a positive or negative DC voltage on top of the reference (V_{ref}=600mV). This provides possibility to periodically reverse the polarity of DC bias in a very slow time-interleaved manner. The voltage noise of the V_{ref} is common-mode noise which is cancelled in the first order at the TIA input since V_{ref} is also used to drive the bias electrode (Fig. 16). The input current noise PSD of the GSR channel is derived as follow:

$$\overline{i_{n,GSR}^2} = \overline{i_{n,CG}^2} + \frac{\overline{v_{n,DAC}^2}}{R_S^2} + \frac{\overline{v_{n,OPA}^2}}{R_f^2} \quad (3)$$

where R_S is the equivalent resistance of the GSR, $V_{n,DAC}$ is the noise of differential voltage ΔV, which is only a fraction of V_{ref}. Thanks to the DEM, the 1/*f* noise of the CG is again reduced for improved GSR sensitivity. To reduce the inaccuracy of ΔV, the V-DAC (Fig. 17) utilizes resistor-based V-I and I-V converters. Hence, ΔV is determined by the ratio of resistors and thus the resistance spread due to PVT variation is compensated.

D. Photoplethysmogram (PPG) Mode

PPG is an optical method to measure heart rate and blood oxygen saturation (e.g. SpO_2). It works by shining light into the tissue where the light will be modulated by the blood volume and oxygenation levels. Similar as GSR mode, the PPG readout also needs a large dynamic range. The DC component of the PPG is dominated by the light absorption of skin tissue, while the AC component of PPG represents the volumetric changes in blood in each peripheral circulation. Hence, the TIA (Fig. 18) works in a similar way as in GSR mode. A photodiode [18] outputs a typical current (I_{PPG}) of ~1µ-25µA_{pp} in which only 1-5% is the actual AC component. Based on the estimated range of input current (I_{PPG}), the CG is reconfigured to a similar level (I_{dc}) for DC current compensation. This partially reduces the net input current flowing to the TIA to improve its dynamic range. The pulse width of LED is 250µS with a programmable duty cycle of 5-50% (Fig. 18).

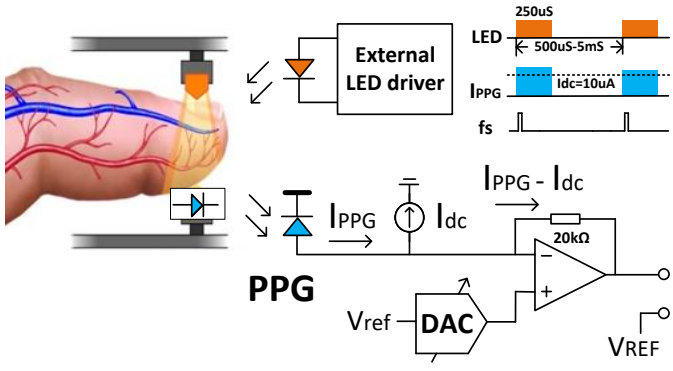

Fig. 18. PPG acquisition mode

E. Analog and Digital Signal Processing

A 12b low-power SAR ADC based on fringe-based capacitors DAC [19] digitizes the output of preamplifier (Fig. 17). Thanks to the fringe capacitor array and the dynamic circuitry, the ADC

has an effective number of bits (ENOB) of 10.4b and consumes 102nW at the default sampling rate of 4kS/s. The ADC power dissipation scales linearly proportionally to its sampling rate and increases to 128µW at 5MS/s.

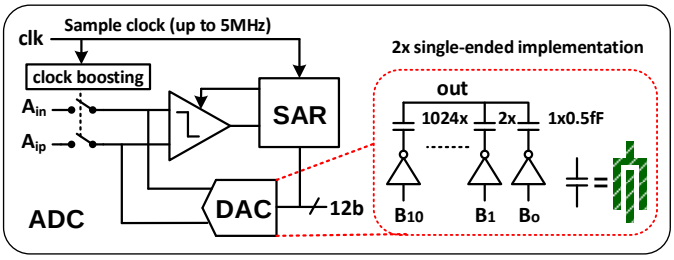

Fig. 19. 12-bit low-power SAR ADC with fringe capacitor-based DAC [19]

The following digital filter chain (Fig. 2) includes a cascaded integrator-comb (CIC) filter, a digital accumulator (ACU), and a finite impulse response (FIR) filter. The digital filters and the ADC provide flexible selection of bandwidth (BW) and sub-sampling rate up to 128*4096 for each mode.

III. Measurement Results

The IC is implemented in TSMC 0.18µm CMOS process. Fig. 20 shows the chip photograph including 3x R-AFE channels and 3x ADCs to facilitate simultaneous, multimodal bio-signal measurement. Each R-AFE (including an ADC) occupies a chip area of 1.1mm^2.

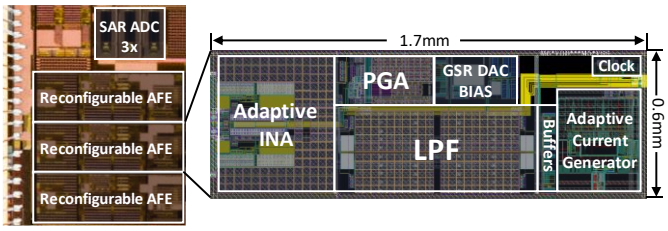

Fig. 20. Chip photograph (3x R-AFE channels)

A. IC Performance

Fig. 21 shows measured ECG channel gain with differential mode (1mV$_{pp}$) and common-mode (300mV$_{pp}$) input signals, respectively. This plot indicates a CMRR of about 100dB over the bandwidth of 200Hz.

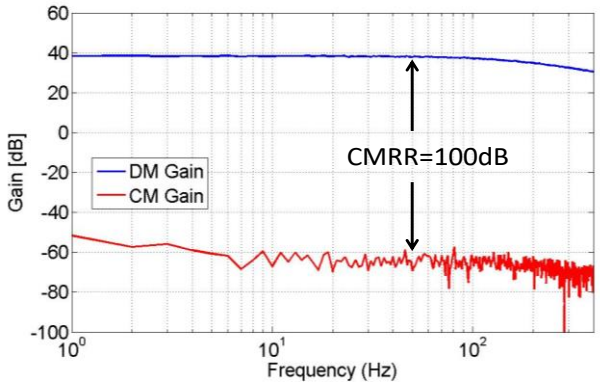

Fig. 21. ECG channel gain and CMRR (with LPF enabled)

Fig. 22 shows the ECG input referred noise at the gain of 88. This noise is measured at the ADC output thus it reflects the total voltage noise of the channel and the 256Hz BW defined by the FIR filter. The chopping frequency at 4kHz is beyond the IA's initial 1/*f* noise corner. This ensures a voltage noise density of 80nV/√(Hz) down to 0.5Hz after chopping.

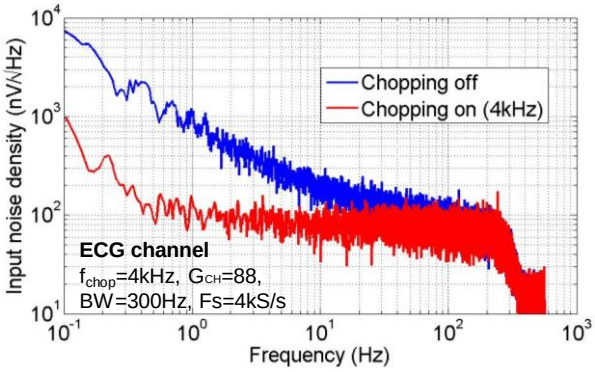

Fig. 22. Input referred noise of the ECG channel

In BioZ mode, 20µA$_{pp}$ and 80µA$_{pp}$ square wave currents at 32kHz were applied in succession to a 100Ω test resistor, which is a typical BioZ value. The input referred voltage noise derived from the channel output includes both the noise of the readout and the CG. When I_{CG}=20µA$_{pp}$ and the DEM is activated, BioZ input noise is 100nV/√Hz at 0.4Hz (Fig. 23), corresponding to a 10mΩ/√Hz impedance sensitivity. When I_{CG} is increased to 80µA$_{pp}$, however, the residual 1/*f* noise is more dominant. This is because the reference current of the CG also suffers from 1/*f* noise, which is not chopped off by the DEM.

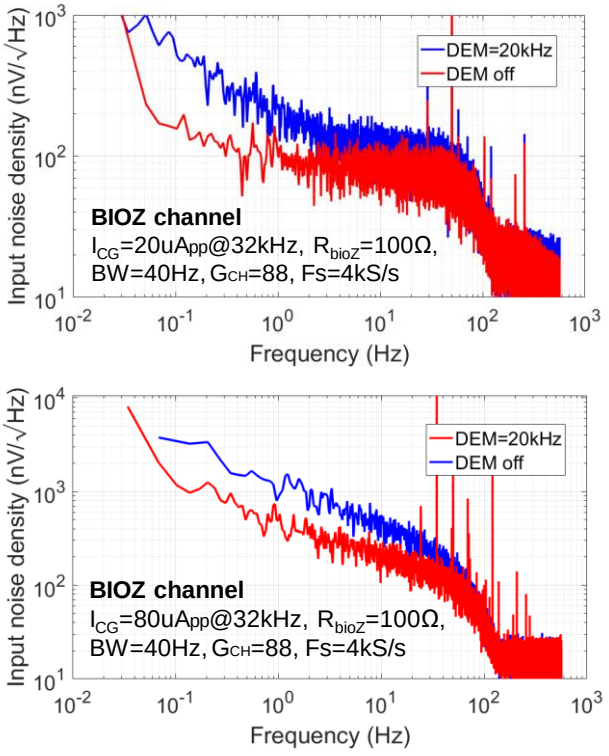

Fig. 23. Input referred noise of the BioZ channel, including the CG noise. (top) I_{CG}=20µA$_{pp}$. (bottom) I_{CG}=80µA$_{pp}$.

In GSR mode, Fig. 24 shows the TIA's input referred current

noise density with various feedback resistors. As expected, the current noise is reduced with a large feedback resistor, which is subject to a reduced dynamic range. For typical GSR equivalent resistance between 50k-500kΩ, the input current noise (at 1Hz) are 40pA/√Hz and 1nA/√Hz. These noise levels correspond to a GSR sensitivity of 0.6μS/√Hz and 10μS/√Hz, respectively.

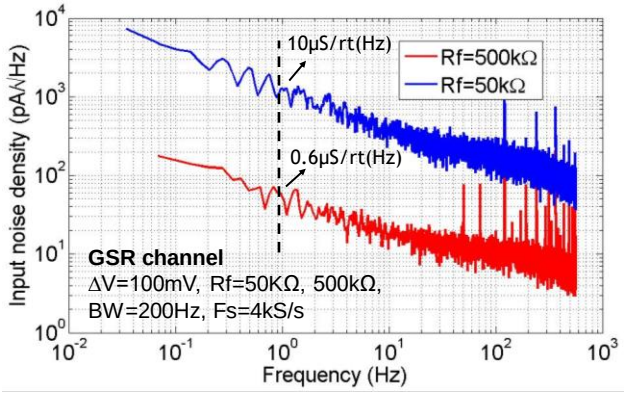

Fig. 24. Input referred noise of the GSR channel (including V-DAC)

In GPA DC-coupling mode, the IA is bypassed and the PGA is chopped at 2kHz. The GPA channel shows an input voltage noise density of 850nV/√Hz (Fig. 25) at the channel gain of 8.

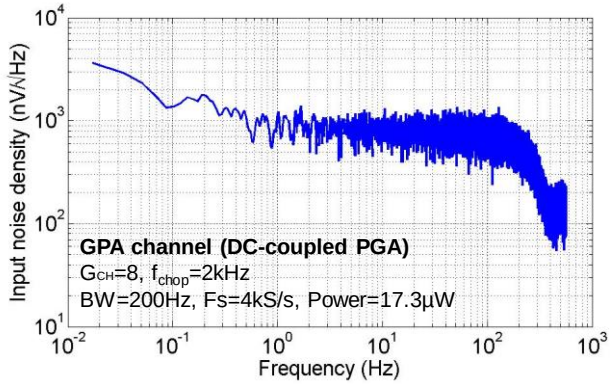

Fig. 25. Input referred noise of the GPA channel (PGA as input stage)

B. System Performance

This section shows simultaneous measurement of multimodal physiological signals via the R-AFEs. In Fig. 26, BioZ (top) and ECG (bottom) are simultaneously measured on the subject's chest with the same recording electrodes. The BioZ plot clearly indicates the respiratory rate of approximately 5 seconds. When the subject was holding his breathing, the respiratory BioZ is almost flat and the impedance cardiography (ICG) is obvious.

Fig. 27 shows the simultaneously recorded thoracic BioZ and finger GSR. The BioZ plot indicates the rate and strength of respiration. The GSR plot shows that the skin conductance only responses to the deep breathing, not the normal breathing. This is expected result because deep breathing and exhaling induce a phasic sympathetic discharge and so more sweating, which is reflected by GSR change.

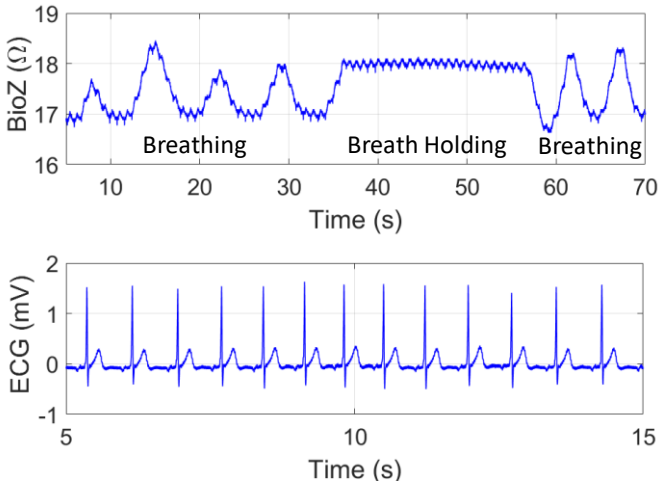

Fig. 26. Simultaneous measurement of respiratory BioZ and (zoom-) ECG

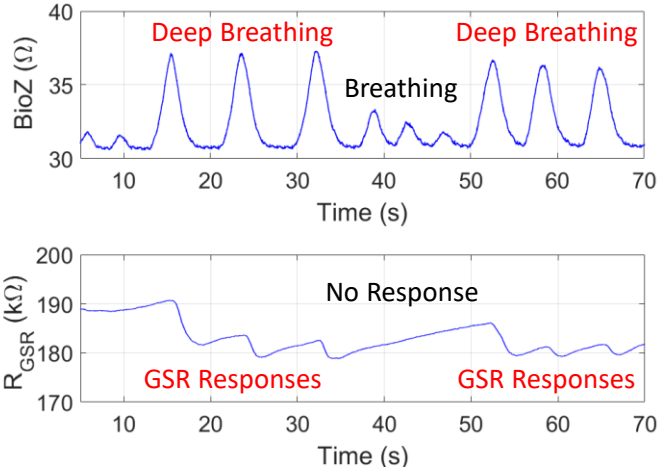

Fig. 27. Simultaneous measurement of thoracic BioZ and finger GSR

The low noise feature of ECG channel makes it suitable for general biopotential signals measurement. Fig. 28 presents the results of scalp EEG recording with Ag/AgCl electrodes. Alpha activities at 10Hz is clearly distinguished between eyes-open and eyes-closed periods.

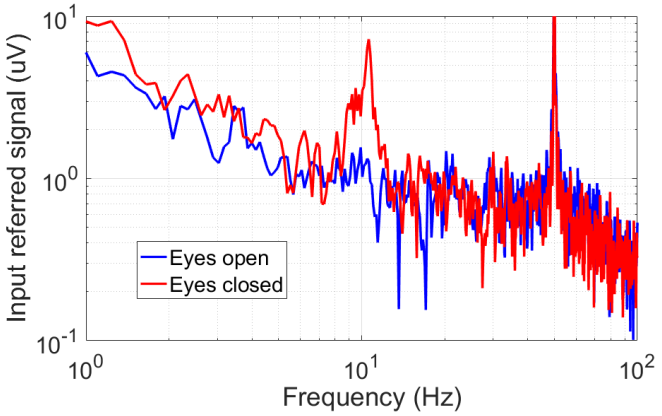

Fig. 28. Spectrum of scalp EEG measurement

Fig. 29 shows the PPG (low-pass filtered at 16Hz) measured from the index finger and the ECG concurrently obtained from the chest, both signals clearly show the same heart rate.

TABLE I COMPARISON TABLE

	ADS1292R [1]	JSSC'15 [2]	JSSC'16 [4]	ESSCIRC'15 [5]	JSSC'14 [6]	Sensors'16 [7]	This work
Technology	N/A	0.18µm	0.18µm	0.18µm	0.35µm	0.13µm	0.18µm
Supply voltage	3V	1.8	1.2V	1.8V	1.8V	1.2	1.2V
Reconfigurable	No	No	No	No	Yes	Yes	Yes
ECG noise (100Hz BW)	1.2µV$_{rms}$	36nV√Hz	0.6µV$_{rms}$	0.6µV$_{rms}$	7.7µV$_{rms}$	1µV$_{rms}$	0.8µV$_{rms}$
GSR/PPG noise	N/A	N/A	36pA$_{rms}$ (4Hz)	N/A	N/A	260pA$_{rms}$ (100Hz)	82pA$_{rms}$ (4Hz)
BioZ noise	40mΩ$_{pp}$ (I_{CG}=30µA$_{pp}$)	4.9mΩ	3mΩ√Hz (I_{CG}=100µA$_{pp}$)	100mΩ$_{pp}$ (I_{CG}=100µA$_{pp}$)	N/A	N/A	10mΩ/√Hz (I_{CG}=20µA$_{pp}$)
BioZ current generator	30µA$_{pp}$ 32k/64kHz	10-400µA$_{pp}$ 100-100kHz	50-200µA$_{pp}$ 20k/40kHz	1-100µA$_{pp}$ 1k-125kHz	N/A	N/A 5k-1MHz	10-200µA$_{pp}$ 1k-1MHz
CMRR@50Hz	105dB	N/A	110dB	62dB	N/A	N/A	100dB
ADC	24b SDM	14b SDM	15b SDM	12b SAR	12b SAR	12b SAR	12b SAR
Power/channel (excl.CG)	335µW (ECG) 335µW (BioZ)	53.4mW (full ASIC)	49µW (ECG) 46µW (BioZ) 15µW (GSR)	31µW (ECG) 155µW (BioZ)	28.4µW	52µW	33µW (ECG) 36µW (BioZ) 20µW (GSR) 17.3µW (GPA)
Area/channel*	N/A	~1.5mm^2 (BioZ)	~5.8mm^2 (ECG)	<1mm^2	~2.7mm^2	~9.3mm^2	1.1mm^2

*based on the area estimation the building blocks shown in chip photographs

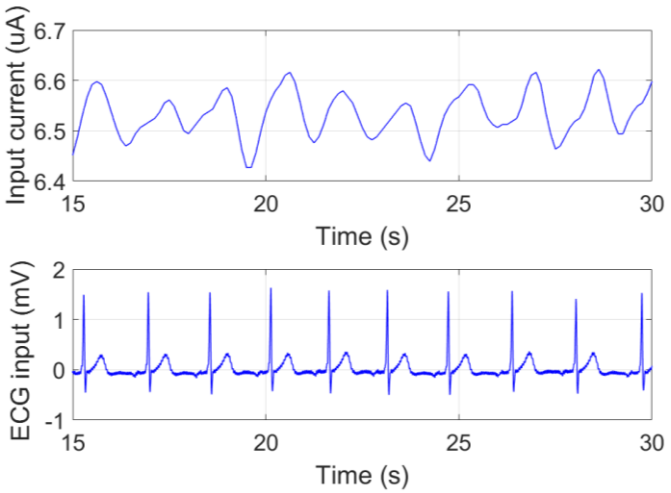

Fig. 29. Heart beats measured in simultaneous ECG/PPG mode

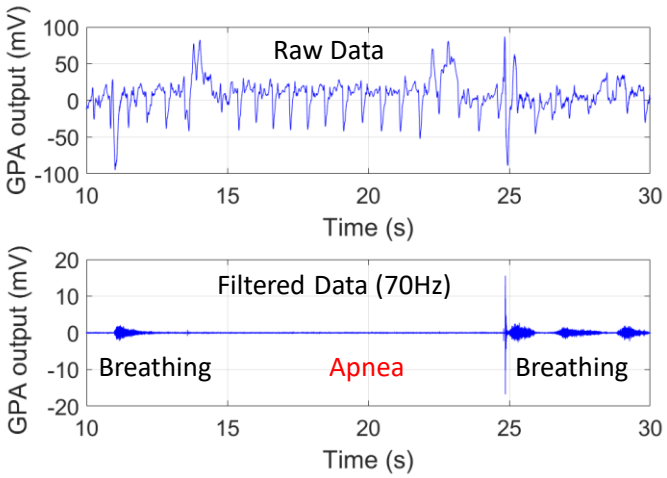

Fig. 30. Tracheal sound including an apnea

The GPA channel is interfaced with two contact microphones [23] to record internal body sounds. To measure tracheal sound, one microphones was placed on the right side of the neck and another one was on the back. Fig. 30 and Fig. 31 show the raw and high-pass filtered (at 70Hz) outputs of the GPA channel. Apnea (Fig. 30 at 25s) and normal respiration (Fig. 31) of the subject are easily recognized.

Table I compares the R-AFE with state-of-the-art dedicated ECG and BioZ readout [1][2], multi-sensor readout [4][5], and R-AFE [6][7]. The proposed R-AFE utilizing dynamic circuit techniques has achieved very competitive performance (ECG noise, BioZ sensitivity and CMRR) to the dedicated ECG/BioZ ICs and the multi-sensor ICs, but with 10x lower power than [1][2][5] and approximately 5.3x smaller channel area than [4]. Compared to other R-AFEs, this work consumes similar power but with ~10x lower noise than [6] and roughly ~8.4x smaller channel area than [7]. Compared to all these prior art works, the proposed R-AFE supports the most types of sensing modalities.

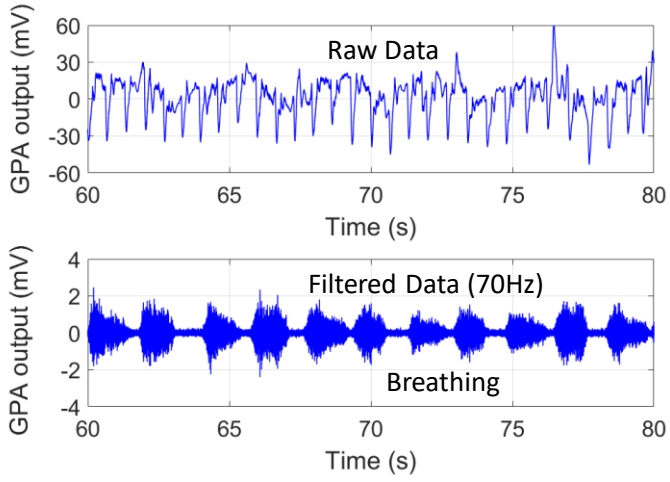

Fig. 31. Tracheal sound indicating respiration

IV. Conclusion

A highly reconfigurable AFE is proposed for wearable and miniaturized cardiovascular and respiratory signals acquisition. The AFE occupies an area of 1.1mm^2 and supports five sensing modes including ECG, BioZ, GSR, PPG and GPA. The AFE advances state-of-the-art dedicated biomedical readouts with a smaller area while outperforming other reconfigurable ICs with improved noise-power tradeoff.

References

[1] TI-ADS1292R, http://www.ti.com/lit/ds/symlink/ads1292r.pdf

[2] S. Hong et al., "A 4.9mΩ sensitivity mobile electrical impedance tomography IC for early breast-cancer detection system," *IEEE J. Solid-State Circuits*, vol. 50, no. 1, pp. 245-257, Jan. 2015.

[3] L.Sant, A. Fant, S. Stojanović, S. Fabbro, J. L. Ceballos, "A 13.2b optical proximity sensor system with 130 klx ambient light rejection capable of heart rate and blood oximetry monitoring," *IEEE J. Solid-State Circuits*, vol. 51, no. 7, pp. 1674-1683, July. 2016.

[4] M. Konijnenburg et al., "A battery-powered efficient multi-sensor acquisition system with simultaneous ECG, BIO-Z, GSR, and PPG," *Digest of ISSCC*, pp.480-482, Feb. 2016.

[5] J. Xu, P. Harpe, J. Pettine, C. Van Hoof, R. F. Yazicioglu, "A low power configurable bio-impedance spectroscopy (BIS) ASIC with simultaneous ECG and respiration recording functionality," *Digest of ESSCIRC*, pp. 396-399. Sept. 2015.

[6] Y. J. Huang et al., "A self-powered CMOS reconfigurable multi-sensor SoC for biomedical applications," *IEEE J. Solid-State Circuits*, vol. 49, no. 4, pp.851-866, April. 2014.

[7] J. Kim and H. Ko., "Reconfigurable multiparameter biosignal acquisition SoC for low power wearable platform," Sensors, 16(12), Dec. 2016

[8] IEC 60601-2-47, Medical electrical equipment - Part 2-47: Particular requirements for the basic safety and essential performance of ambulatory electrocardiographic systems

[9] J. Xu et al., "A 36μW reconfigurable analog front-end IC for multimodal vital signs monitoring," *Symposium on VLSI Circuits*, pp. 170-171, June. 2017.

[10] C. Enz, G.C. Temes., "Circuit techniques for reducing the effects of op-amp imperfections: autozeroing, correlated double sampling, and chopper stabilization," *Proceedings of the IEEE*, 84 (11), pp.1584-1614, 1996.

[11] K.A.A. Makinwa, "Dynamic offset cancellation techniques in CMOS," *ISSCC Tutorial*, Feb. 2007

[12] S. C. Au, D. Maes, and C. F. Rahim, "Body grabbing switch," *US Patent 6008689*. Maxim Integrated Products, Inc.

[13] R. Hogervorst, J. P. Tero, R. G. H. Eschauzier, J. H. Huijsing, "A compact power-efficient 3 V CMOS rail-to-rail input/output operational amplifier for VLSI cell libraries" *IEEE J. Solid-State Circuits*, vol. 29, pp. 1505 – 1513, Dec 1994.

[14] AAMI ES1, "Safe current limits for electromedical apparatus," 1993.

[15] I. F. Triantis, A. Demosthenous, M. Rahal, H. Hong, R. Bayford, "A multi-frequency bioimpedance measurement ASIC for electrical impedance tomography", *Proc. of ESSCIRC*, pp.331-334. Sept. 2011.

[16] H. Ko, T. Lee, J. Kim, J. Park, J. P. Kim., "Ultralow-power bioimpedance IC with intermediate frequency shifting chopper," *IEEE Trans. on Circuits and Systems II*, vol. 63, no. 3, pp. 259-263, Mar. 2016.

[17] H. Ha et al., "A bio-impedance readout IC with frequency sweeping from 1k-to-1MHz for electrical impedance tomography," *Symposium on VLSI Circuits*, pp. 174-175, June. 2017.

[18] OSRAM SFH 7050 - Photoplethysmography Sensor, https://www.osram-os.com/Graphics/XPic8/00219349_0.pdf/SFH%207050,%20Lead%20(Pb)%20Free%20Product%20-%20RoHS%20Compliant.pdf

[19] P. Harpe, Y. Zhang, G. Dolmans, K. Philips, H. de Groot, "A 7-to-10b 0-to-4MS/s flexible SAR ADC with 6.5-16fJ per conversion-step," *Digest of ISSCC*, pp.472-474, Feb. 2012.

[20] M. van Elzakker et al., "A 10-bit charge-redistribution ADC consuming 1.9μW at 1MS/s," *IEEE J. Solid-State Circuits*, vol. 45, no 5, pp. 1007-1015, May. 2010.

[21] C. C. Liu, S. J. Chang, G. Y. Huang and Y. Z. Lin, "A 10-bit 50-MS/s SAR ADC with a monotonic capacitor switching procedure," *IEEE J. Solid-State Circuits*, vol. 45, no. 4, pp. 731–740, April 2010.

[22] M. Ding et al., "A 5.5fJ/conv-step 6.4MS/s 13b SAR ADC utilizing a redundancy facilitated background error-detection-and-correction scheme," *Digest of ISSCC*, pp. 460-461, Feb. 2015.

[23] BIOPAC,TSD108, https://www.biopac.com/product/contact-microphone